Interpretation of ion-channeling spectra in ion-implanted Si with models of structurally relaxed point defects and clusters

Giorgio Lulli,* Eros Albertazzi, Marco Bianconi, and Alessandra Satta
Consiglio Nazionale delle Ricerche-Istituto per la Microelettronica e i Microsistemi, Sezione di Bologna, Via P. Gobetti 101, I-40129 Bologna, Italy

Simone Balboni
CeSIA-Settore Reti e Comunicazioni, Università di Bologna, Viale Filopanti 3, I-40126 Bologna, Italy

Luciano Colombo
INFM–SLACS Sardinian Laboratory for Computational Material Science and Dipartimento di Fisica, Università di Cagliari, Cittadella Universitaria, I-09042 Monserrato (CA), Italy

(Received 18 December 2003; published 29 April 2004)

We investigate the application of atomistic models of self-interstitial defects to the simulation of Rutherford backscattering-channeling (RBS-C) spectra in ion irradiated Si. By the comparison of simulated and experimental measurements, we verify the ability of different models, either of elementary interstitials or of small clusters, to reproduce experimental spectra measured under different alignment conditions in Si lightly damaged by Si^+ ion implantation. A model system for RBS-C simulation is built by inserting a distribution of defects in a supercell with size of $\sim 10^6$ atoms. The system is then structurally relaxed by the application of the classical environment-dependent interatomic potential (EDIP). After adjusting the defect distribution in order to fit the $\langle 100 \rangle$ RBS-C spectrum, simulations are performed under the other alignment conditions investigated. The scattering factors of defects are then extracted from both experimental and simulated RBS-C spectra and compared. It is shown that the anisotropy of experimental damage is not compatible with a significant presence of random (incoherent) disorder, but can be reproduced by some of the defect models under consideration: the split-$\langle 110 \rangle$ interstitial, the diinterstitial formed by the addition of an interstitial to the split-$\langle 110 \rangle$ interstitial, and two different configurations of the four-interstitial aggregate; one formed by two close diinterstitials and the other by the aggregation of four split-$\langle 100 \rangle$ interstitials. Due to the different $\langle 100 \rangle$ scattering factors of the four defect configurations which are found to reproduce experimental spectra, there is an inherent uncertainty of a factor of 2 in the estimate of the amount of interstitials by $\langle 100 \rangle$ RBS-C analysis. The agreement between simulations and experiments is remarkable, considering that the method makes use of physical, although empirical, models of defects, where the only adjustable parameter is the absolute concentration of interstitials.

DOI: 10.1103/PhysRevB.69.165216 PACS number(s): 61.85.+p, 61.72.Ji, 82.80.Yc, 61.80.Jh

I. INTRODUCTION

The introduction of impurities and lattice defects in crystalline Si by charged particle irradiation is a process widely used to modify the technologically relevant properties of the material. Improving the understanding and control of the transformations induced by this process has been for many years the main driving force for the investigation of radiation defects in Si.

The Rutherford backscattering-channeling (RBS-C) technique[1] has been used for decades to characterize radiation damage in Si. One distinctive feature of RBS-C is the possibility to identify atomic location of defects and host impurities by performing measurements under varying beam-target alignment conditions. In this case Monte Carlo (MC) simulation of ion-channeling spectra[2–5] is often used for determining the location of atoms displaced from regular lattice sites. In previous studies of ion-implanted Si, results have been explained with the assumption that radiation damage is in the form of split-$\langle 110 \rangle$ (I_S) interstitials.[4,6–9] Early examples of this interpretation date back to more than 20 years ago.[6,7] More recently, discussing MC simulation of ion implantation in Si, it was found that modeling the accumulated damage as either I_S or random (but not for instance tetrahedral) defects allowed good simulation of the channeling tails in as-implanted dopant profiles.[8] Furthermore, our previous reports on atomistic MC simulations of RBS-C spectra using elementary point defects[10–12] have shown that modeling the damage as I_S interstitials structurally relaxed by empirical potentials reproduced well multiaxial RBS-C measurements of lightly damaged Si, whereas the assumption of hexagonal (I_H), tetrahedral (I_T), or random configurations of defects did not. The effect of defect induced strain on the response of RBS-C measurements, which had been addressed mainly qualitatively in the past,[13,4,14] was fully included in our approach; we could therefore show that modeling the lattice relaxation around defects was a prerequisite to obtain good agreement with experiments.

Notwithstanding these results, it may be questioned if a model based on simple point defects can be a reasonable approximation of the disorder produced by ion implantation. It is commonly believed that elementary point defects are mobile in Si at room temperature;[15] therefore we would expect that only point defect aggregates, complexes, or amorphous clusters are stable in room temperature (RT) as-implanted Si. While there is wide agreement on the

configurations and energetics of elementary interstitials in Si, the situation is quite different in the case of self-interstitial clusters, for which many configurations have been proposed in the literature. The purpose here is not to discuss the theoretical models of defects, but rather to investigate the possibility of interpreting RBS-C measurements in ion-implanted Si with atomistic models of small self-interstitial clusters. This is pursued by comparing experimental RBS-C spectra and spectra simulated with a MC binary collision approximation (MC-BCA) code modified to include atomistic models of defects. We show how simulations are sensitive to the atomic configurations of defects and determine what among the proposed configurations can actually reproduce experiments within the uncertainties of the method. Our previous results[10] have shown that the influence of vacancy defects, which induce a disorder much less effective on the RBS-C response than the one of interstitials, is of minor importance. We will therefore focus on Si self-interstitials, choose some candidate configurations of small clusters I_n, with the number n of excess Si atoms in the range 1–4, introduce them in the simulation of RBS-C spectra, and compare simulations and experimental measurements.

II. EXPERIMENT

A (100) float zone *n*-type 500Ω cm Si wafer was implanted at room temperature with 180 keV Si^+ ions at a dose of 10^{14} cm^{-2}. These conditions produce a disorder distribution fully contained within a depth of 700 nm and with maximum defect concentration of the order of a few atomic percent. The thickness of the profile makes it possible to analyze both the direct scattering and the dechanneling properties of radiation defects using standard RBS-C analysis, while the low disorder level allows us to stay within the relatively simple assumption of weakly interacting defects.

RBS-C measurements were performed using a 2 MeV He^+ beam and backscattering angle of 170° under the seven axial ⟨111⟩, ⟨112⟩, ⟨113⟩, ⟨100⟩, ⟨130⟩, ⟨120⟩, ⟨110⟩ and the two planar {110} and {100} alignments.

Details of the measurement setup, which includes a Faraday chamber for absolute measurements (uncertainty in the yield ~2%), are reported in Ref. 16. Spectra of reference virgin and thick ion-amorphized Si samples were always measured together with spectra of implanted samples.

III. COMPUTER SIMULATION

A. Building Si supercells containing structurally relaxed defects

The procedure to introduce structurally relaxed point defects in the simulation of RBS-C spectra has been described previously.[10] We have added here the possibility of including small self-interstitial cluster I_n, with the number n of excess Si atoms (EA's) in the range 1–4. Figure 1 shows the ball-and-stick models of some of the defects used in the present work. The initial coordinates of the defective atoms (DA's) which form each cluster were taken from the results of tight-binding molecular-dynamics calculations performed in 512-atom Si cells.[17] Besides EA's, DA's (dark gray balls in Fig. 1) include also the lattice atoms which, as a consequence of the introduction of extra Si atoms, undergo large displacement from their bulk positions, forming bonds with EA's. I_1 (we will refer to it as either I_1 or I_S in the following) is the well-known split-⟨110⟩ interstitial, composed of two fourfold coordinated DA's; I_2 (composed of three fivefold coordinated DA's) derives from the addition of one single interstitial to an I_1 defect; I_3 (composed of four sixfold coordinated DA's) derives from the addition of another single interstitial to the I_2 structure, which gives origin to a tetrahedral cage symmetrically embedded into the crystalline environment; I_{4a} is formed by two close I_2 defects. All these configurations are obtained with a ⟨110⟩ dumbbell defect being the fundamental nucleation catalyst. A different concept is the one behind I_{4b} (composed of eight fourfold coordinated DA's), which is formed by the agglomeration of four split-⟨100⟩ interstitials on the {100} plane.[18–21] Its underlying building principle is that Si atoms must preserve their fourfold coordination. For comparison purposes, RBS-C simulations were also performed using I_H and I_T configurations of elementary interstitials.

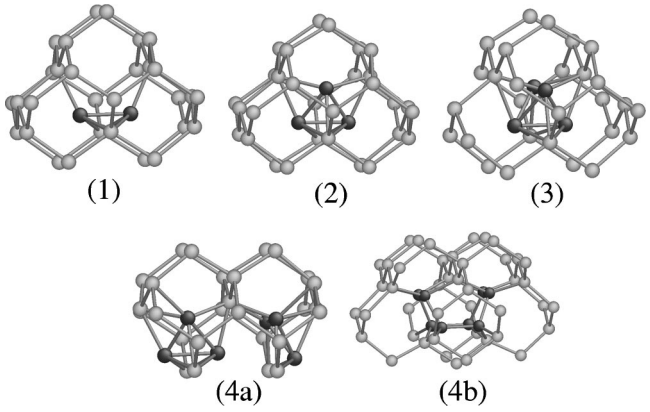

FIG. 1. Ball-and-stick models of the self-interstitial defects used for the simulation of RBS-C spectra: (1) elementary split-⟨110⟩ (I_1 or I_S), (2) diinterstitial (I_2), (3) triinterstitial (I_3), (4a) model *a* of four-interstitial cluster (I_{4a}), and (4b) model *b* of four-interstitial cluster (I_{4b}) (see text for more details on the structural models). The defect configurations, produced for illustrating purposes, have been generated in a Si cell (10×10×10) lattice units and relaxed with the EDIP potential. Si defective atoms (DA's) are dark gray, whereas bulklike atoms are light gray. Figures were produced by the free software ATOMEYE (Ref. 33). The configurations of elementary hexagonal (I_H) and tetrahedral (I_T) interstitials, also used in this work for the simulation of RBS-C spectra, are not reported.

The model sample for the simulation of RBS-C spectra was prepared as follows. A Si supercell containing about 2.2×10^6 atoms (12×12×1900 lattice units, the long side corresponding to the [001] direction perpendicular to the wafer surface) was populated using only one kind of defect at a time, according to a depth distribution profile given in input. The interstitial concentration investigated in this work was in the range 1–3 % atomic fraction. A depth profile of single vacancies, equal to the one of EA's, was inserted to balance the total number of EA's. The exact defect locations at a

certain depth were chosen at random, taking into account all the possible orientations of defects in the Si lattice and under the constraint that cluster-vacancy, cluster-cluster, and vacancy-vacancy distances were the largest compatible with the local concentration of defects. These minimum distances depend on the defect type and concentration; in our case they varied between 4 and 5 Å. The constraint on mutual distances minimizes the interactions which can modify the number and type of defects upon relaxation, thus ensuring that the simulated RBS-C response is characteristic of a well-defined defect type.

An energy minimization procedure at constant volume and using periodic boundary conditions was applied to the supercell (more details on the procedure can be found in Refs. 10 and 22). In this work we have used the EDIP (Refs. 23 and 24) empirical potential, which is known to give a good description of local bonding in bulk defects and disordered phases of Si. For a discussion of the influence of the model potentials on the results obtained for single interstitials, the reader is referred to Ref. 10. We mention that, from the point of view of the response of the RBS-C simulations, the results obtained with environment-dependent interatomic potential (EDIP) were very similar to those obtained with the Tersoff[25] III potential. On the other hand, we observed that some of the defect clusters reported in Fig. 1 (I_2, I_3, and I_{4a}) were not stable when using the Stillinger-Weber[26] potential for relaxation.

B. Simulation of RBS-C spectra

RBS-C spectra of the relaxed supercells with defects were simulated with the computer code BISIC,[5,16] in which full calculation of He^+ trajectories is performed according to the MC-BCA method. Using the concept of close encounter probability[2] and approximating the path of a backscattered ion with a straight trajectory, the program calculates the yield at the detector as a function of backscattering energy. A description of the program can be found in Ref. 16. As a preliminary step, we verified that simulations accurately reproduced reference spectra of undamaged and thick amorphous Si samples measured under all beam-sample orientations investigated. For comparison purposes, RBS-C simulations of ion-implanted Si were performed using also the random model of damage. In this case a self-interstitial/vacancy pair is created by displacing an atom at random from its lattice site, without introducing any distortion in the surrounding crystal. This model, although unphysical, is important as a reference, being used in the two-beam approximation,[27] the standard method for the extraction of disorder profiles from RBS-C spectra.

Since RBS-C analysis of (100) Si is typically performed under the $\langle 100 \rangle$ alignment, as a first step we determined the depth distribution of interstitials which reproduces the experimental $\langle 100 \rangle$ RBS-C spectrum for each of the defect models investigated. Figure 2 shows the example of the fitting obtained in the case of elementary I_S defects. Damage distributions as obtained by the fitting of the experimental $\langle 100 \rangle$ RBS-C spectrum were then used for the simulation of spectra under the other alignment conditions.

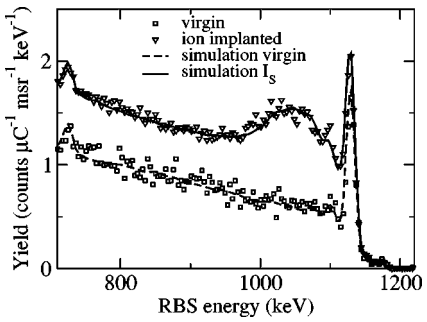

FIG. 2. Experimental and simulated RBS-C spectra of virgin and RT ion irradiated Si (180 keV Si^+ ions, dose 10^{14} Si cm^{-2}). The simulation of the ion irradiated sample is the one done with the model of single split-$\langle 110 \rangle$ (I_S) point defects, using the interstitial depth profile labeled I_S in Fig. 3.

A source of uncertainty of the method is the uncertainty in the configuration of defects as optimized by the EDIP potential. The direct application of more exact *ab initio* or semiempirical quantum mechanical calculations to a system as large as our simulation supercells is clearly not feasible. To investigate the sensitivity of RBS-C simulation to the defect optimization method, we developed a procedure for using *ab initio* optimized I_S within the RBS-C simulation. We chose I_S because it is known to be reliably optimized by a first-principles method. The purpose is to compare the results obtained with the EDIP-I_S and those we have found out introducing quantum mechanical effects in the model of the defect. In order to reach this goal, we performed calculations within the framework of the local-density-functional theory (DFT-LDA), using norm-conserving pseudopotentials[28] and a 16 Ry kinetic-energy cutoff. The geometry of I_S was fully relaxed[29] in a periodically repeated supercell containing 216 lattice sites. The Brillouin zone was sampled using the Γ point. A cluster containing the defect and a number of neighboring atoms sufficient to include the strained region which gives nonnegligible contribution to the ion backscattering yield was then extracted from the small cell and used to populate the large RBS-C supercell. In order to preserve the structure optimized with DFT-LDA, no relaxation was applied to the supercell before RBS-C simulation. The limit of this procedure is that, in order to avoid overlapping of the strained regions around DFT-I_S, the maximum allowable concentration of defects is quite low (0.8–0.9 %). This makes such a ''cut-and-paste'' approach not feasible for the simulation of our experimental sample, which has a maximum defect concentration of the order of 1–2 %. Therefore the procedure was just used for the comparison test, performed on a model system populated by a uniform 0.89% atomic concentration of DFT-I_S. The concentration of I_S in the EDIP relaxed supercell was first adjusted to give the same $\langle 100 \rangle$ RBS-C yield of the DFT-I_S. A slightly smaller concentration (0.82%) was necessary, thus indicating a slightly higher scattering efficiency of the EDIP-I_S in the $\langle 100 \rangle$ alignment. The yields (not shown) of the spectra simulated with the two defect models under all other axial and planar alignment conditions and using the two concentrations above were equal within $\pm 6\%$. This result demonstrates that

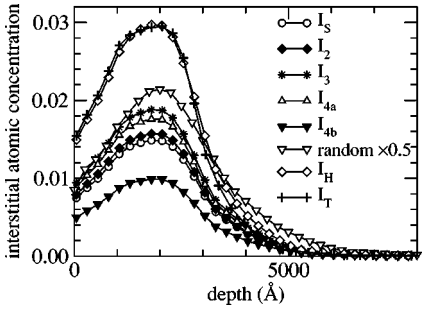

FIG. 3. Concentration depth profiles of self-interstitials, or EA's, resulting from the fit of the experimental ⟨100⟩ RBS-C spectrum (Fig. 2) with the different models of defects investigated.

EDIP-I_S and DFT-I_S models show very similar behavior from the point of view of RBS-C analysis.

IV. RESULTS AND DISCUSSION

A. Determination of defect distributions

Figure 3 shows the depth distribution profiles of self-interstitials, or EA's, resulting from the fitting of the experimental ⟨100⟩ RBS-C spectrum with the different defect models investigated. As mentioned above, each fitting is performed using only one kind of defects at a time. The differences among the curves, which may reach a factor 4, depend on the different ⟨100⟩ scattering efficiencies of defects: the higher the number of interstitials needed, the lower the scattering efficiency of defects under the ⟨100⟩ alignment. On the other hand, the shapes of the distributions are practically the same, except from the profile of random defects which is somewhat different from all the others.

Concerning random defects, we had already observed[10] that they have a much lower ⟨100⟩ scattering efficiency than I_S interstitials; this is due to the fact that in one I_S defect there are actually two DAs, and also to the strain induced in the neighborhood of I_S by lattice relaxation. A low ⟨100⟩ scattering efficiency is observed also for I_H and the I_T interstitials. This is mainly a consequence of the ⟨100⟩ alignment; in fact, both defects are strongly shadowed by the ⟨100⟩ Si rows. Actually, as pointed out in Ref. 10, most of their ⟨100⟩ yield is due to the distortion they induce in the surrounding lattice. Their scattering efficiency is much higher under other alignment conditions investigated, such as the ⟨110⟩. On the opposite end there is the I_{4b} cluster, whose scattering efficiency in the ⟨100⟩ alignment is significantly higher than the one of all other defects. Again, this is an effect of the orientation; in fact, this defect displays a relatively lower scattering efficiency under other orientations, such as, the ⟨110⟩ (see results in the following section).

The above results clearly show that the absolute concentration of EA's extracted from the ⟨100⟩ RBS-C spectrum depends on the damage model. This is due both to the specific structural properties of each defect and to the fact that the ratio between DA's and EA's varies with the defect model. In fact, RBS-C is mainly sensitive to the amount of atoms heavily displaced from lattice sites, i.e., DA's.

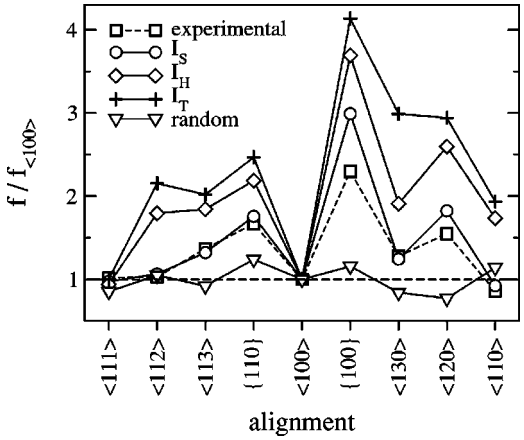

FIG. 4. Scattering factors of defects in the different alignment conditions, normalized to the scattering factor in the ⟨100⟩ orientation ($f/f_{\langle 100\rangle}$), extracted from experimental spectra and from spectra simulated with three different configurations of point defects: split-⟨100⟩ (I_S), hexagonal (I_H), and tetrahedral (I_T) self-interstitials. The signature of the random defect model is reported for comparison.

Given the high number of defect models and orientations investigated, some data reduction procedure is needed to synthesize the comparison of experiments and simulations. To this purpose we have extracted the defect scattering factors (f, as defined in the basic theory of defect induced ion dechanneling[1]) at the depth of the damage peak ($\sim$200 nm according to Fig. 2) from the spectra simulated under the nine alignment conditions and for each defect model, and have normalized these values to the scattering factor in the ⟨100⟩ orientation ($f_{\langle 100\rangle}$). The $f/f_{\langle 100\rangle}$ has been calculated also for the experimental spectra, and the comparison of simulated and experimental $f/f_{\langle 100\rangle}$ has been reported and discussed in the following section. The procedure to extract $f/f_{\langle 100\rangle}$ from RBS-C spectra is described in the Appendix. The trend of $f/f_{\langle 100\rangle}$ as a function of beam-target orientation can be considered as a characteristic signature of defects.

B. Results of multiaxial analysis

Figure 4 shows the experimental $f/f_{\langle 100\rangle}$ and the $f/f_{\langle 100\rangle}$ extracted from the simulations performed with three configurations of point defects, I_S, I_H, I_T, and the random defect model. Since the random defect is spatially isotropic, its $f/f_{\langle 100\rangle}$ should be exactly=1 for all orientations. The average is actually close to 1, but, due to statistical and procedural errors, the points deviate from this value. Their standard deviation ($\sim$16%) may be considered as an empirical estimate of the uncertainty of the data reduction procedure. Also, by definition, $f/f_{\langle 100\rangle}=1$ for the ⟨100⟩ alignment.

The large difference between the experimental signature and the signature of the random defect demonstrates the anisotropic nature of damage. A consequence is that amorphous or incoherent defect clusters should be a minor component of disorder. It is also evident that among the possible configurations of fully relaxed point defects, only I_S displays a signature in agreement with the experiment.

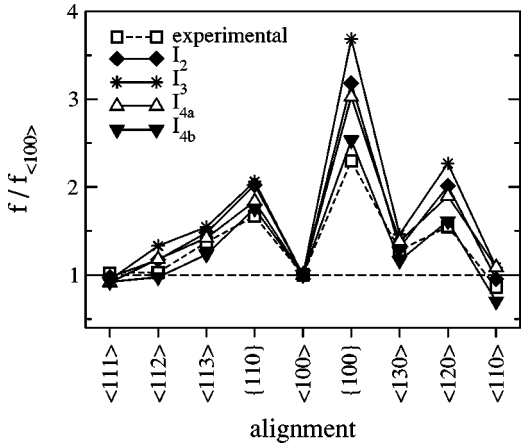

FIG. 5. Scattering factors of defects in the different alignment conditions, normalized to the scattering factor in the $\langle 100\rangle$ orientation ($f/f_{\langle 100\rangle}$), extracted from experimental spectra and from spectra simulated with different models of self-interstitial clusters: di-interstitial (I_2), tri-interstitial (I_3), and the two different configurations of the four-interstitial aggregate (I_{4a} and I_{4b}) reported in Fig. 1.

In Fig. 5 the experimental $f/f_{\langle 100\rangle}$ is compared with the $f/f_{\langle 100\rangle}$ values extracted from the simulations performed with the different I_n ($n=2-4$) shown in Fig. 1. Here all the defects display similar signatures, each following more or less closely the trend of the experiment. The similarity is observed not only for defect configurations which have I_S as building unit (I_2, I_3, and I_{4a}), but also for I_{4b}, which, as pointed out in the preceding section, is based on a different building criterion. Notwithstanding the similar qualitative trends of the signatures, significant differences in the quantitative results exist. They are better pointed out in Table I, where the relative differences of experimental and simulated $f/f_{\langle 100\rangle}$ values have been reported for all defect models and alignment conditions investigated (except for the $\langle 100\rangle$, for which, by definition, $f/f_{\langle 100\rangle}=1$). The last column of Table I reports the overall standard deviations of the various defect models from the experiment, which measure the ability of each defect to reproduce the full set of experimental data. Defects have been ordered from the smallest to the largest value of the overall standard deviation. If we compare these overall deviations with the accuracy of the method, which has been estimated to be about 16%, we conclude that the deviations of I_S, I_{4b}, I_{4a}, and I_2 signatures are within or close to the uncertainty of the procedure, whereas those of I_3, random defect, I_H, and I_T are clearly out. Among defects which have I_S as a basic building block, I_3 is the only one which appears in significant disagreement with the experiment. It is worth noting that I_{4b}, which obeys a building criterion different from the one of I_S, is the defect which gives the best overall fit of multiaxial data.

These results indicate that there is not a unique defect model compatible with experiments. We recall that in the present approach the absolute concentration of EA's is an adjustable parameter, which may significantly vary depending both on the defect model and on the beam-target alignment. For example, both I_{4b} and I_{4a} defects are compatible with experiments, although giving absolute concentrations of EA's, as fitted on the $\langle 100\rangle$ RBS-C spectrum, which differ by a factor ~ 2. Further work will be necessary to examine more defect configurations, in order to better understand the sensitivity and selectivity of the method.

It must be pointed out that the above results depend on the specific implantation condition investigated. The nature of disorder, described as small point defect aggregates, and the apparent absence of amorphous clusters are probably the consequence of a process dominated by self-annealing and clustering of highly mobile defects under implantation. The important role of self-annealing is evident if we compare the maximum concentration of point defects determined in our analysis (1–2 at. %, depending on the defect type) and the maximum atomic concentration of defects calculated with MC-BCA simulation of the ion-implantation process. In fact, using either TRIM (Ref. 30), or our simulation code KING,[31] and setting a threshold energy of atomic displacement of 13 eV, we found a maximum defect concentration of about 15% for an implant of 180 keV, 10^{14} Si^+ cm^{-2}.

Since there is practical interest to extend the atomistic RBS-C simulation to samples implanted at higher doses, and/or with higher mass ions, it will be important to investigate whether RBS-C spectra of more heavily damaged Si can be simulated simply by increasing the concentration of point

TABLE I. Differences (in percent) between $f/f_{\langle 100\rangle}$ extracted from experimental RBS-C spectra and $f/f_{\langle 100\rangle}$ extracted from spectra simulated according to different defect models, under the different channeling conditions investigated. The last column reports, for each defect, the overall standard deviations of data. Defects are ordered from the lowest to the highest values of the overall standard deviation.

	$\langle 111\rangle$	$\langle 112\rangle$	$\langle 113\rangle$	$\{110\}$	$\{100\}$	$\langle 130\rangle$	$\langle 120\rangle$	$\langle 110\rangle$	σ
I_{4b}	−9.6	−5.5	−10.1	+5.2	−6.2	+10.1	+4.0	−18.7	10.6
I_{1S}	−4.4	+3.5	−3.5	+5.4	+30.2	−2.9	+17.7	+7.6	13.6
I_{4a}	−10.5	+14.6	+3.7	+10.1	+31.7	+7.9	+22.4	+26.5	19.3
I_2	−4.6	+14.0	+8.0	+21.2	+38.5	+2.5	+29.8	+11.0	21.0
I_3	−7.6	+29.2	+12.7	+23.6	+60.4	+14.0	+46.3	+26.3	34.0
Random	−16.2	+2.0	−32.8	−25.6	−49.6	−34.2	−50.1	+32.8	36.5
I_{1H}	−7.8	+74.4	+34.5	+31.1	+60.7	+49.1	+67.5	+102.0	63.7
I_{1T}	−1.9	+109.2	+47.4	+47.9	+79.9	+133.6	+89.8	+125.2	95.5

defects and small aggregates, or if different models of elementary damage units will be required to that purpose. One key feature for the extension of the method is the behavior of the empirical potential in describing the structural changes which occur in heavily damaged Si as a consequence of the interactions between closely spaced defects.

V. CONCLUSIONS

RBS-C multiaxial analysis of Si implanted at RT with low-medium dose 180 keV Si^+ ions indicates that ion induced disorder is strongly anisotropic, and therefore not compatible with a significant presence of amorphous clusters. Atomistic simulation of RBS-C spectra shows that most of the small aggregates (1–4 interstitials) having the split-$\langle 110\rangle$ defect as a basic building unit, when relaxed with the classical EDIP potential, reproduce, within the uncertainty of the procedure, the defect scattering factors extracted from experimental spectra under a wide range of alignment conditions. The only case in significant disagreement with experiments is I_3. Also I_{4b}, although based on the aggregation split-$\langle 100\rangle$, shows good agreement with experiments. On the other hand some of the defect models investigated (I_3, I_H, I_T) are not compatible with RBS-C measurements. This fact indicates either that these defects are not present in significant amount in the irradiated sample or that their structural model is not correct. It is worth recalling that in the present method, contrary to a usual practice in atomic location, we do not adjust the position of atoms to fit RBS-C spectra. Defect configurations result from geometrical optimization with the EDIP potential and are consistent with a physical, although empirical, model of defects. The only adjustable parameter is the absolute concentration of interstitials. Considering the defect configurations which are compatible with experiments, this concentration varies by a maximum factor 1.8 between the defects which display the lowest (I_{4a}) and the highest (I_{4b}) scattering efficiencies in the $\langle 100\rangle$ alignment. This factor is an estimate of the maximum uncertainty in the absolute concentration of EA's obtained by our atomistic RBS-C analysis.

ACKNOWLEDGMENTS

Thanks are due to S. Cristiani and R. Lotti for ion implantation and technical assistance in RBS-C measurements. This work was supported by the FIRB national project (Contract No. RBAU01LLX2).

APPENDIX: EXTRACTION OF DEFECT SCATTERING FACTORS FROM RBS-C SPECTRA

To compare the results of multiaxial measurements and simulations we make use of the defect scattering factor *f*, a characteristic property of defects as described in the basic channeling theory.[1,27] In the framework of the two-beam formulation, for a given axial or planar direction, the normalized RBS-C yield of a layer containing a concentration depth profile of defects $n_d(z)$ is given by

$$\chi(z)=\chi_R(z)+[1-\chi_R(z)]\frac{n_d(z)}{N}f, \tag{A1}$$

where N is the atomic density of the crystal, f is the defect scattering factor (for randomly displaced atoms, $f=1$ under all alignment conditions), and $\chi_R(z)$ the dechanneled fraction of the beam, which, in the single-scattering regime, can be approximated by

$$\chi_R(z)=\chi_V(z)+[1-\chi_V(z)]\{1-\exp[-\sigma I(z)]\}. \tag{A2}$$

In Eq. (A2) $\chi_V(z)$ is the normalized yield of the spectrum of the virgin crystal, σ is the defect dechanneling cross section and $I(z)=\int_0^z n_d(t)dt$ is the integral of defects from the surface to the depth *z*. Equation (A2) holds for low concentration of defects (integral of defects $\lesssim 10^{17}$ cm^{-2}). From the dechanneling induced in 2 MeV He^+ ions by a thin amorphous Si on Si crystalline substrate,[32] it is possible to estimate $\sigma \simeq 3\times 10^{-19}$ cm^2. Under this condition in Eq. (A2) we can approximate $\{1-\exp[-\sigma I(z)]\}\simeq \sigma I(z)$.

To estimate f at the position of the damage maximum from Eq. (A1), we need $\chi_R(z)$, and to calculate $\chi_R(z)$ from Eq. (A2) we need $\sigma I(z)$. At a depth z_0 sufficiently large, $n_d(z_0)\simeq 0$ [Eq. (A1)] and $\chi(z_0)\simeq\chi_R(z_0)$, i.e., the measured yield corresponds to $\chi_R(z_0)$. We can therefore use Eq. (A2) to extract σ, which is given by

$$\sigma=\frac{\chi_R(z_0)-\chi_V(z_0)}{[1-\chi_V(z_0)]I}, \tag{A3}$$

where now I is the integral of the whole defect depth profile. Note that in the case of simulated spectra, $n_d(z)$ and I are known, the former corresponding to the profile used to calculate the RBS-C spectrum. On the other hand, for the experimental spectrum $n_d(z)$ and I are unknown. We have seen in Sec. IV A (Fig. 3) that the integrals of the different depth profiles deduced from the simulations with different defect models may vary, but their shape is almost the same. We can reasonably assume a similar shape for the ''true'' $n_d(z)$ of the experimental spectrum: in this way the ratio $I(z)/I$ can be evaluated at any depth. Substituting σ from Eq. (A3) in Eq. (A2) this ratio is just what is necessary to calculate $\chi_R(z)$.

We can finally calculate the defect scattering factor as

$$f=\frac{N}{n_d(z)}\left[\frac{\chi(z)-\chi_R(z)}{1-\chi_R(z)}\right]. \tag{A4}$$

f depends on the concentration of defects and on the alignment condition. As described in Sec. IV A, we chose the $\langle 100\rangle$ experimental spectrum as the reference for fitting the depth profiles of different defects (see Fig. 3). Therefore, to get rid of the dependence of f on defect concentration we simply normalize all scattering factors to the one obtained for the $\langle 100\rangle$ alignment ($f_{\langle 100\rangle}$).

The variation of $f/f_{\langle 100\rangle}$ as a function of the crystallographic alignment can be considered as the signature of the defects in the sample.

*Electronic address: lulli@bo.imm.cnr.it

[1] L.C. Feldman, J.M. Mayer, and S.T. Picraux, *Material Analysis by Ion Channeling* (Academic Press, New York, 1982).
[2] J.H. Barrett, Phys. Rev. B **3**, 1527 (1971).
[3] P.J.M. Smulders and D.O. Boerma, Nucl. Instrum. Methods Phys. Res. B **29**, 471 (1987).
[4] B. Weber, E. Wendler, K. Gärtner, D.M. Stock, and W. Wesch, Nucl. Instrum. Methods Phys. Res. B **118**, 113 (1996).
[5] E. Albertazzi, M. Bianconi, G. Lulli, R. Nipoti, and M. Cantiano, Nucl. Instrum. Methods Phys. Res. B **118**, 128 (1996).
[6] G. Götz and G. Sommer, Radiat. Eff. **41**, 195 (1979).
[7] K. Morita and D. Carstasnjen, Radiat. Eff. **59**, 117 (1981).
[8] G. Hobler, Nucl. Instrum. Methods Phys. Res. B **96**, 155 (1995).
[9] G. Otto, G. Hobler, and K. Gärtner, Nucl. Instrum. Methods Phys. Res. B **202**, 114 (2003).
[10] S. Balboni, E. Albertazzi, M. Bianconi, and G. Lulli, Phys. Rev. B **66**, 045202 (2002).
[11] G. Lulli, E. Albertazzi, M. Bianconi, and S. Balboni, Nucl. Instrum. Methods Phys. Res. B **211**, 50 (2003).
[12] M. Bianconi, E. Albertazzi, S. Balboni, and G. Lulli, Nucl. Instrum. Methods Phys. Res. B (to be published).
[13] P. Sigmund, Appl. Phys. Lett. **14**, 114 (1969).
[14] G. Lulli, M. Bianconi, A. Parisini, S. Sama, and M. Servidori, J. Appl. Phys. **88**, 3993 (2000).
[15] M. Lannoo and J. Bourgoin, *Point Defects in Semiconductors (I)* (Springer-Verlag, Berlin, 1981).
[16] G. Lulli, E. Albertazzi, M. Bianconi, G.G. Bentini, and R. Lotti, Nucl. Instrum. Methods Phys. Res. B **170**, 1 (2000).
[17] L. Colombo, Annu. Rev. Mater. Res. **32**, 271 (2002).
[18] N. Arai, S. Takeda, and M. Kohyama, Phys. Rev. Lett. **78**, 4265 (1997).
[19] M. Kohyama and S. Takeda, Phys. Rev. B **60**, 8075 (1999).
[20] B.J. Coomer, J.P. Goss, R. Jones, S. Öberg, and P.R. Briddon, J. Phys.: Condens. Matter **13**, L1 (2001).
[21] D. Pierreux and A. Stesmans, Phys. Rev. B **68**, 193208 (2003).
[22] S. Balboni, Ph.D. thesis, University of Bologna, Bologna, Italy, 2002.
[23] M.Z. Bazant, E. Kaxiras, and J.F. Justo, Phys. Rev. B **56**, 8542 (1997).
[24] J.F. Justo, M.Z. Bazant, E. Kaxiras, V.V. Bulatov, and S. Yip, Phys. Rev. B **58**, 2539 (1998).
[25] J. Tersoff, Phys. Rev. B **38**, 9902 (1988).
[26] F.H. Stillinger and T.A. Weber, Phys. Rev. B **31**, 5262 (1985).
[27] E. Bøgh, Can. J. Phys. **46**, 653 (1968).
[28] G. Bachelet, D. Hamann, and M. Schlüter, Phys. Rev. B **26**, 4199 (1982).
[29] These calculations were performed using the plane-wave self-consistent-field PWSCF code: http://www.pwscf.org
[30] J.F. Ziegler, J.P. Biersack, and U. Littmark, *The Stopping and Range of Ions in Solids* (Pergamon, New York, 1985).
[31] G. Lulli, E. Albertazzi, M. Bianconi, R. Nipoti, M. Cervera, A. Carnera, and C. Cellini, J. Appl. Phys. **82**, 5958 (1997).
[32] M. Bianconi, R. Nipoti, M. Cantiano, A. Gasparotto, and A. Sambo, Nucl. Instrum. Methods Phys. Res. B **84**, 507 (1994).
[33] J. Li, Modell. Simul. Mater. Sci. Eng. **11**, 173 (2003).